RESEARCH PAPER



Assessment of the stress path and prediction of fault activity in oil reservoirs (Ahvaz oil field)

Behrouz Teimouri ¹, Mehran Arian ^{1,*} ¹, Mohammad Abdideh ², Ali Solgi ¹, Zahra Maleki ¹

Received: 25 November 2024, Revised: 25 February 2025, Accepted: 10 March 2025 © University of Tehran

Abstract

Understanding fault conditions and slip behavior is essential throughout the lifespan of a reservoir. The formation of new gaps or faults within a reservoir significantly increases the costs and risks associated with drilling operations. This research examined the potential for fracture formation resulting from discharge and a reduction in pore pressure. Well drilling data from a reservoir in southwest Iran were used to calculate the principal stresses and develop a geomechanical model. Based on this model, the safe mud weight window for drilling was also determined. Finally, the potential for fracture and fault formations was assessed throughout the reservoir's production phase. The results show that the mud loss pressure in the reservoir corresponds to the minimum horizontal stress value (σ 3), with an average value of approximately 41.75 MPa. The stress regime in the reservoir is a normal ($\sigma v > \sigma H > \sigma h$), and the safest drilling direction is parallel to the vertical stress. According to the results, the orientations of the minimum and maximum horizontal stresses are N16W-S16E and N74E-S74W, respectively, with a standard deviation of 6.5 degrees. As a result of the production and discharge of hydrocarbon reservoirs, the initial pore pressure decreases. The decrease in pore pressure causes a change in the effective stress and subsequently the in situ stress field, and this phenomenon will cause new fractures and faults in the reservoir. The formation of new faults due to reservoir discharge is more likely to occur in the sandstone layers of the studied reservoir compared to the limestone and dolomite layers.

Keywords: Stress Field; Fault; Pore Pressure; Geomechanical Model; Zagros.

Introduction

For many years, rock mechanics (geomechanics) has been applied in different sectors of the global oil industry, including hydraulic fracturing, underground gas storage, sand production wells, subsidence of the earth's surface or the sea floor, activation of faults, change in permeability, productivity wells, and increased production from heavy oil reservoirs. In fact, numerous projects have been established to address these topics. In other words, rock mechanics, or geomechanics, in petroleum engineering focuses on the effect of rock stress and resistance on the behavior of formations affected by reservoir activity (Ashena et al. 2022).

Geomechanical modeling of a reservoir is a critical objective for developing effective reservoir management strategies. This modeling serves as the foundation for other geomechanical studies, including wellbore stability analysis, hydraulic fracturing operations, safe mud weight window design, and assessing the potential for fault formation due to production. The one-dimensional geomechanical model is the simplest type of geomechanical

¹ Department of Earth Sciences, SR.C., Islamic Azad University, Tehran, Iran

² Department of Petroleum Engineering, Omidiyeh Branch, Islamic Azad University, Omidiyeh, Iran

^{*} Corresponding author e-mail: mehranarian@yahoo.com

model, representing the state of the stress field and the variations in the physical and mechanical properties of the ground within the reservoir along the well (Abdelghany et al., 2021).

The field of petroleum geomechanics investigates the prediction of rock behavior, compression, failure, and faulting in oil and gas reservoirs as a result of drilling and exploitation. The drop in oil prices and the competitiveness of production from hydrocarbon resources have further highlighted the importance of drilling planning and the exploitation of hydrocarbon reservoirs. During drilling, issues, such as the adhesion of drilling pipes to the well wall, decreased well diameter, weed on the mud, increased well diameter, and blowouts, can escalate costs up to one billion dollars per year in some cases (Taghipour et al. 2021).

The condition of the well walls not only impacts the drilling phase but also plays a critical role during field operations by influencing pore pressure reduction. Wellbore instability can occur at various life stages of a well's lifecycle, including during drilling, well completion, and flow and production testing (Khodami et al., 2021). These instabilities are a major source of drilling problems, leading to increased costs, time delays, and, in some cases, the complete loss of the well (Radwan and Sen 2021). Oil companies invest significant time and resources in addressing problems arising from wellbore instability during drilling operations. Estimates regarding the financial losses caused by wellbore instability vary, but they are generally approximated around 1 billion dollars per year. Therefore, studying this issue is essential to mitigate the costs associated with oil wellbore instability.

Many parameters can influence the wellbore instability, including those related to the properties of drilling mud and its interaction with the formation, as well as the mechanical properties of the formation and the orientation of stresses surrounding the well. In general, the wellbore instability can be attributed to physicochemical and mechanical factors, or a combination of both (Farsimadan et al., 2020).

To predict the safe and drilling mud weight intervals for future wells and to better understand the parameters affecting wellbore instability, it is essential to develop a geomechanical model. A geomechanical model is a logical set containing information related to geology, regional stresses, rock mechanical properties, and pore pressure. It serves as a valuable tool for efficiently updating information relevant to drilling operations and reservoir management (Edress et al., 2021).

From a geomechanical perspective, production and gradual depletion of the reservoir lead to changes within the reservoir. The possibility of gap creation is one of the most important changes resulting from production. Understanding the condition and slippage of these gaps throughout the life cycle and production of a reservoir is crucial. Gaps in drained reservoirs may form in three ways. Production can lead to the creation of faults and fracture in the reservoir (Darvishpour et al., 2019), resulting in depletion and a corresponding decrease in pore pressure. Tectonic faults are distinguished from reservoir faults by their larger dimensions, which make them identifiable in seismic sections, as well as by the presence of earthquake hypocenters with moderate to high magnitudes (Arian et al., 2012). Pore pressure refers to the fluid pressure inside the rock cavities, which supports a portion of the Earth's stress and maintains the pore spaces' openness. A decrease in pore pressure leads to an increase in effective normal stress, and this change can induce elastic deformations throughout the reservoir (Azadpour et al., 2015). When the stress path is sufficiently large and reaches or exceeds the critical stress value, a fault may develop within the reservoir. Sometimes it is necessary to excavate the drained reservoir to access the lower reservoir layers. For example, drilling operations in the Ahvaz oil field located in southwest Iran are conducted after years of extraction from the shallower reservoir to access the deeper reservoir (Abdelghany et al., 2023). Due to the reduction in pore pressure in drained formations, it is necessary to use lower mud weight to prevent cracks and distortions during drilling. To prevent the entry of fluids from higher layers into the well, the mud weight must not fall below a certain threshold. Drilling in drained areas leads to significant changes in the pressure gradient (Bagheri et al., 2021). These changes can cause numerous problems that cannot be addressed using traditional drilling methods. Different methods are used to excavate a drained reservoir. By using a mud weight greater than the minimum principal stress and drilling in the correct direction, it is possible to prevent a hydraulic gap formation near the well (Ashena et al., 2020). The use of additives to prevent mud penetration into the formation, as well as resistant additives to cement the formation grains in the well wall, can also help mitigate some problems. Incorporating loss-preventing materials can help reduce loss fluid loss; however, there have been cases where up to 1,000 barrels of mud were lost despite the use of these agents. Mud pressure management systems also address some issues associated with drained reservoirs. While the use of reinforcing materials can prevent cracks in the well walls, they may have detrimental effects on the formation (Bashmagh et al., 2022). The following are studies by various researchers related to geomechanics and the physics of reservoir rocks.

Anees et al. investigated the role of shear zones and faults in the accumulation of economically viable underground gas reservoirs. They concluded that the fault network serves as a pathway for hydrocarbon migration within the reservoirs (Anees et al., 2022).

The research findings of Ashraf et al. showed that multiple and complex tectonic activities, along with the formation and activity of several normal faults, have led to the development of sedimentary basins in the Tibetan Plateau, China (Ashraf et al., 2024).

Shraf et al. successfully detected the heterogeneity between sand and shale reservoirs using artificial intelligence to analyze rock physics. This method relies on petrophysical parameters and rock physics (Shraf et al., 2020).

Yifan et al. employed the seismic methods to identify the petrophysical properties of the reservoirs, such as porosity and the fluid types, incorporating these findings into the thermoelastic modeling of the reservoir (Yifan et al., 2024).

Qing et al. artificial neural networks can be used to determine the shear resistance parameters of rocks, such as the coefficient of adhesion and internal friction, which can then be applied in elasto-plastic modeling of the rocks (Qing et al., 2024).

Most studies conducted in the field of oil geomechanics are related to the wellbore stability analysis. This study analyzes the well stability and investigates the potential for reservoir fault activity in the reservoir resulting from reduced pore pressure. This perspective will significantly enhance safe drilling and production while reducing costs throughout the life of a well.

The data and information used in this study are derived from various well operations, including logging, geology, and well testing, which were subjected to quality control before modeling.

A significant advantage of this study method is the accuracy of the models generated by utilizing data banks and comprehensive subsurface information. The methodology of this study is designed to utilize the routine data available within the oil industry.

This research aims to employ geomechanical modeling, using data obtained from the reservoir charts to evaluate the potential for fracture formation in the drained reservoir. The goals of the geomechanical investigation into cracking and its propagation in drained reservoirs include:

- 1) Calculating the principal stresses acting on the reservoir rock at various depths.
- 2) Assessing the stress path and critical stress of the rock within the studied reservoir.
- 3) Determining the safe mud window using geomechanical parameters specific to the reservoir.
- 4) Investigating the potential for fractures resulting from reservoir discharge and pore pressure reduction.

According to the petrophysical and well test data collected from the reservoir rock, this study introduces a specific and accessible method for assessing the potential for fracture formation in the drained oil and gas reservoirs.

Geological setting of the Ahvaz oil field

The Ahvaz oil field is located in the Dezful embayment area of Khuzestan Province in the central part of Ahvaz city (southwestern Iran) and exhibits a northwest-southeast trend parallel to the Zagros Mountain range. The Ahvaz oil field extends 67 km in length and 6 km in width. This oil field is bordered by the Ramin oil field to the north, the Maroun oil field to the east, the Shadgan and Mansouri oil fields to the south, and the Abtaimur and Sosangerd oil fields to the west (Figure 1). The Ahvaz oil field features a significant structural formation and is regarded as one of the final sections of the Zagros folded region. This anticline is located on an uplift (horst) formed in older strata and is unconformably located beneath the Ahvaz surface anticline of the Aghajari Formation. The Ahvaz anticline is approximately symmetrical, with its surface at the head of the Asmari formation lying about 2,500 meters below sea level. In the Ahvaz field, this formation comprises sandstone, limestone, and dolomite, with an average porosity of 18%. In the Ahvaz oil field, the API gravities of Asmari oil, Ilam oil, and Sarvak oil are approximately 32.6, 29-, and 26-degrees API, respectively.

The stratigraphic column of the studied oil field is shown in Figure 2. The Asmari Formation serves as the reservoir layer analyzed in this study.

Tectonics and Geology of Dezful embayment

The Zagros Folded-Thrust Belt is part of the Alpine-Himalayan Belt, which is the result of the opening and then closing of the Neo Tethys Ocean between the Central Iranian Microplate and the Arabian Plate (Berberian, 1995). The Zagros Folded-Thrust Belt is divided from the northeast to the southwest into 5 tectonic zones: the Long Zagros Thrust Belt, the Simple Folded Belt, the Zagros Foredeep and the Dezful embayment, the Zagros Coastal Plain, and the Lowlands of the Persian Gulf and Mesopotamia. There are two saddle or hybrid zones in the Zagros Foredeep, the Dezful embayment in Iran and the Kirkuk Subduction in Iraq.

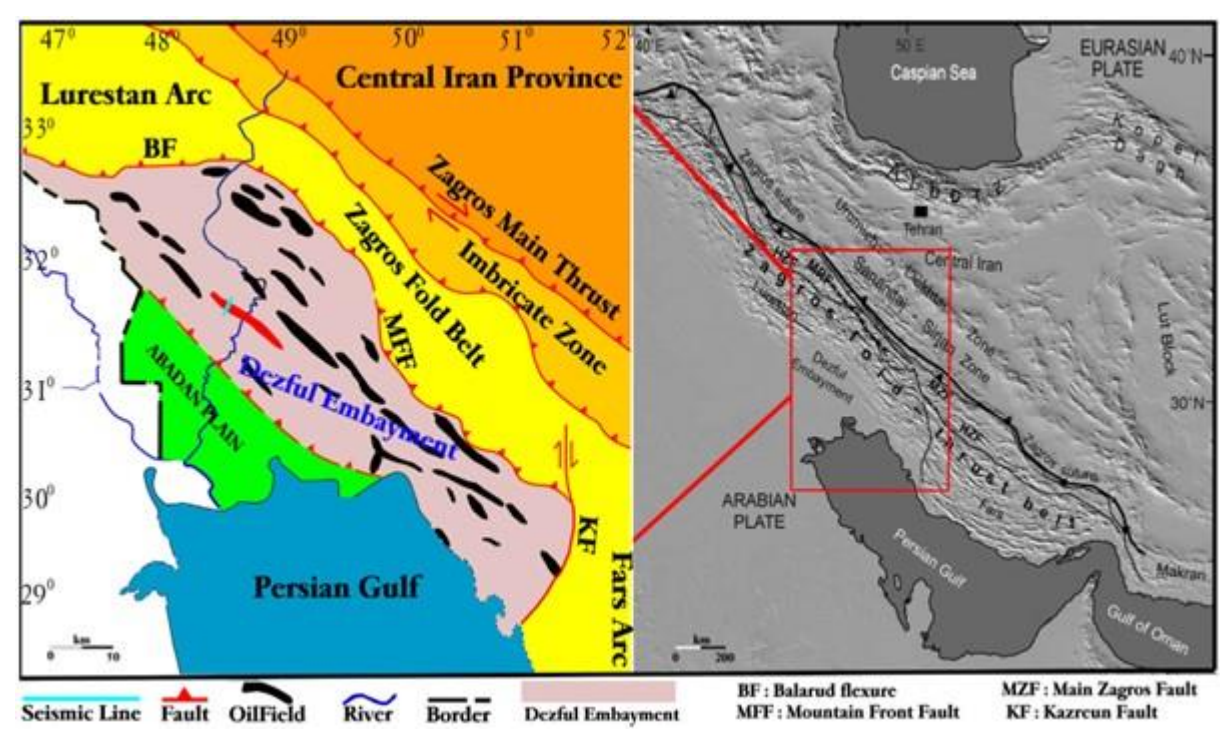


Figure 1. Location of the Ahvaz oil field in southwestern Iran (modified from Hosseini et al., 2015)

Era	Period	Epoch	Formation	Lithology Description	Lithology
Cenozoic	Tertiary	Miocene - Pliocene	Aghajari	Sandstone, Clay stone & Gypsum and Anhydrite	
		M. Miocene	Gachsaran	Anhydrite and Gypsum, Clay stone, Marl, Limestone and Salt	
		Oligocene-Miocene	Asmari	Sandstone, Limestone, Clay stone and Marl	
		U.Paleocene- L.Oligocene Pabdeh	Pabdeh	Argillaceous Limestone, Shale and Marl	
	Cretaceous	Cretaceou Upper	U.Gurpi	Argillaceous Limestone, Shale,	= = = =
			Tarbur	Marl and Limestone	
-			L.Gurpi	23447 4440 24440 444	
Mesozoic			Ilam	Marl, Shale and Limestone	
			Laffan	Shale and Limestone	
			Sarvak	Limestone, Shale	

Figure 2. Stratigraphic column and lithological description of the studied oil field

The Dezful depression is separated from the Izeh zone by the Kohistan and Izeh foreland faults from the northeast and east, respectively, from the Lorestan zone by the Balarud fault from the northeast, from the Abadan plain by the Zagros foreland fault from the southeast, and from the Fars zone by the Kazerun fault from the southeast. Except for the Kazerun fault, the other faults do not have surface outcrops and can be identified using tectonic evidence, earthquake data, and the effect of these faults on the geometry of the folds. These faults, along with the three Haftgel, Hendijan, and Khark-Mish highs, have played a fundamental role in the sedimentation and tectonic evolution of this depression. The geological situation of the Dezful depression is completely different compared to the Izeh and Lorestan zones (Najafi and Lajmorak, 2020). From a stratigraphic point of view, the surface outcrop of the Izeh and Lorestan zones consists predominantly of Cretaceous-Miocene stratigraphic units (Khami Group, Bangestan Group, Pabdeh-Gurpi Formation and Asmari Formation). However, the Dezful embayment surface outcrop consists of Middle Miocene-Pliocene stratigraphic units (Gachsaran, Mishan, Aghajari and Bakhtiari Formations). From a structural point of view, the Izeh and Lorestan zones consist of narrow anticlines with a Zagros trend (northwest-southeast). The height of some of these anticlines reaches more than 300 meters. The core outcrop of the anticlines in the Izeh and Lorestan zones is formed by the Bangestan Group (Ilam-Sarvak) and even older formations. This situation can be seen in anticlines such as Kabirkouh, Anaran, Chenareh, Rit, Gurpi, Payun, Bangestan in the south of the Izeh and Lorestan zones in the vicinity of the Dezful downthrust. A thrust fault is seen in the core of most of these anticlines. This fault often places the Bangestan group formations (Ilam- Sarvak) on the Pabdeh-Gurpi formations. However, in the Dezful downthrust, the Asmari Formation, which forms the resistant whalebone geometry of many Zagros folds and is one of the most important reservoirs in this belt, is exposed only in the core of the Asmari, Dara, and Khaviz mountain anticlines. In this downthrust, the Miocene evaporites of the Gachsaran Formation, which form a very good

cap rock for the Asmari reservoirs, have acted as a main detachment horizon and have caused a change in the geometry and scale of the Dezful downthrust anticlines from surface to depth. This anticline has a much smaller wavelength and amplitude at the surface than at depth. The Dezful embayment anticlines show axial displacement from surface to depth, and their axial surface effect does not coincide from surface to depth. Therefore, the Dezful embayment anticlines have formed large oil traps beneath the Gachsaran Formation. The Dezful embayment has experienced two tectonic positions, pre-deep and above the wedge, in the evolution of the Zagros orogenic basin from the Neogene to the present (Sherkati et al., 2005).

Asmari Reservoir

The Asmari Formation is one of the geological formations of Iran, which is considered the youngest reservoir rock of the Zagros zone, with an age of Late Oligocene (Chatian) to Early Miocene (Aquitanian) (Allahkarampour et al, 2010). The dominant lithology of this formation consists of resistant cream to brown limestones and in some areas such as Ahvaz, sandstone. The Asmari Formation is the richest oil reservoir in Iran and the Middle East and one of the richest carbonate reservoirs in the world. This reservoir rock supplies oil and gas reserves to 62 oil fields, of which 14 super fields and 12 giant fields are classified in the global classification. This formation becomes slightly sandy towards the southwest and towards the mouth of the Persian Gulf, which is called the Ahvaz sands; So that in fields such as Paznan, Ahvaz, Maroon and Mansouri, the Ahvaz sandstone member covers about one third to one quarter of the total thickness of the formation. The Ahvaz sandstone member in the Asmari reservoirs increases the quality of the reservoir and improves the recovery coefficient. This reservoir in northwest Lorestan is formed from the Kalhor evaporite sediments. Most of the porosity and permeability of this formation is related to the porosity resulting from fracture.

Materials and methods

In this research, the geomechanical model of the well (MEM) was first designed to determine the behavior and resistance parameters of the reservoir rock, including elastic coefficients, as well as the stress field affecting the reservoir at the studied depth. Also, the safe mud window for the well was designed and analyzed. Of note, the potentials for fault creation due to reservoir production and discharge were examined by determining the stress path and identifying the critical value for normal fault creation using established relationships. Figure 3 shows the flowchart of the geomechanical analysis steps.

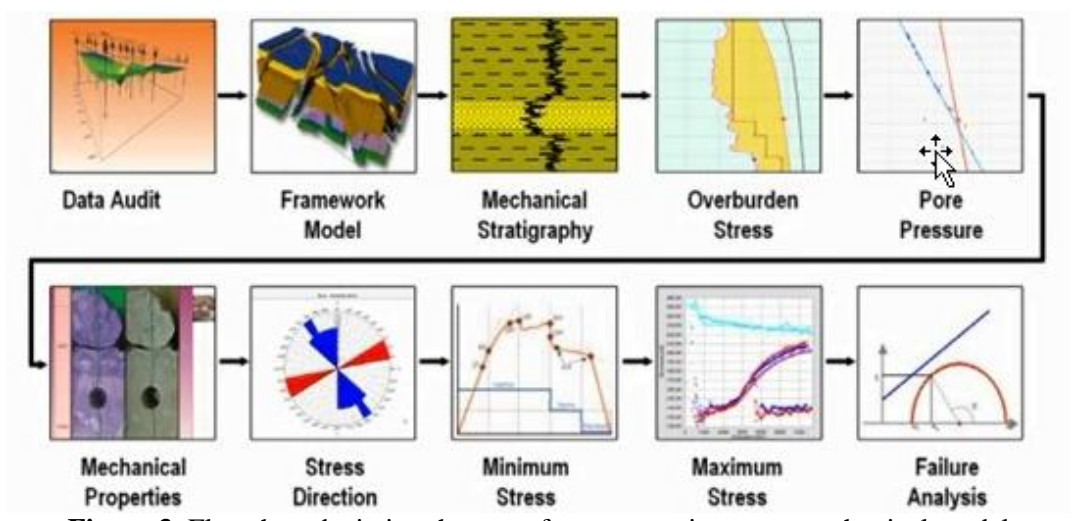


Figure 3. Flowchart depicting the steps for constructing a geomechanical model

Petrophysical information

The first step in constructing and analyzing a geomechanical model is to gather petrophysical data, which includes essential information such as various log data, drilling reports, and core samples. These data should possess specific characteristics, including accessibility and general applicability across various drilling wells, while also being capable of representing a wide range of reservoir rock parameters. Among the most important of these data with the aforementioned characteristics are the petrophysical data obtained from graphing operations or well logging. Petrophysical log based on their characteristics offers valuable information, such as specific resistance in different zones, porosity, fluid type, density, lithology, and numerous other parameters derived from these factors. These parameters can be used to create various diagrams and charts, and in certain cases, they can facilitate discussions on the well trajectory and different ranges concerning reservoir quality and productivity (Hoseinpour and Riahi 2022).

This research uses the logs of gamma ray, density, and shear and pressure wave sonic logs obtained from a well in the Asmari Formation in Ahvaz oil field.

Mechanical earth model (MEM)

To construct a mechanical earth model and determine the in situ stresses and the mechanical characteristics of the reservoir, the elastic moduli of the reservoir rock must be calculated dynamically at all specified depths. The elastic moduli of the reservoir rock are obtained using Relationships 1 (Mohammed, 2017).

1- Young's modulus: longitudinal deformation of rock samples in response to applied stress

$$Ed = \frac{\rho b \left[3 - 4 \left(\frac{\Delta t c}{\Delta t s} \right)^2 \right]}{\Delta t s^2 - \Delta t c^2} \tag{1}$$

2- Shear modulus: changes in the rock angle due to the application of shear stresses

$$Gd = \frac{\rho b}{\Delta t s^2} \tag{2}$$

3-Poisson's ratio: the ratio of changes in the cross-sectional area to the change in the length of the sample

$$\nu = \frac{\frac{1}{2} \left(\frac{\Delta ts}{\Delta tc}\right)^2 - 1}{\left(\frac{\Delta ts}{\Delta tc}\right)^2 - 1} \tag{3}$$

To calculate the elastic moduli, the required data include the RHOB, DTc, and DTs. The log RHOB provides the density value (ρ), while the shear wave travel time is derived from Δ ts or DTs, and the compressional wave travel time is obtained from Δ tc or DTc. Poisson's ratio is dimensionless, whereas the units of the other elastic moduli are in gigapascal (GPa).

For the next calculations, the elastic moduli derived in dynamic mode must be converted to static mode, which can be achieved using empirical relationships specific to the same oil field (Table 1).

In this research, the uniaxial compressive strength (UCS) of the rock was assessed using the experimental relationships, as outlined in Equation 4 (Han et al., 2019).

$$UCS = e^{-0.633 + \frac{246.540}{\Delta t}} \tag{4}$$

Rock Properties	Dynamic	Static
Young's modulus	$\frac{\rho b \left[3 - 4 \left(\frac{\Delta t c}{\Delta t s} \right)^2 \right]}{\Delta t s^2 - \Delta t c^2}$	0.4145E _{dyn} -1.0593
Shear modulus	$rac{ ho b}{\Delta t s^2}$	$\frac{Esta}{2(1+vsta)}$
Poisson's ratio	$\frac{1/2\left(\frac{\Delta ts}{\Delta tc}\right)^2 - 1}{\left(\frac{\Delta ts}{\Delta tc}\right)^2 - 1}$	$0.7 \times \nu$

Table 1: The experimental relationships for converting dynamic to static moduli (Mohammed, 2017)

The tensile strength of the rock, T, varies between UCS/8 and UCS/12, depending on the formation type. For the studied reservoir, its value is calculated using Equation 5.

$$T = \frac{UCS}{10} \tag{5}$$

Results and Discussion

MEM output is depicted in Figures 4, 6, and 7.

The overall diagram illustrating the aforementioned modules as a function of depth can be derived by calculating the values of the dynamic modules, as shown in Figure 4.

The Young's modulus diagram, which represents the hardness of the rock (Figure 4), shows higher values at both beginning and end sections of the well, particularly in areas where the reservoir rock is limestone. Moreover, the tolerance threshold of the reservoir rock in these areas exceeds the applied stresses, reducing the likelihood of fractures and faults occurring.

The Poisson's ratio diagram (Figure 4) indicates that the variations in this modulus, which reflects the characteristics of the rock, are more pronounced in the initial and final sections of the well compared to other areas, primarily due to the changes in the rock type within the formation. Formations exhibiting a higher Poisson's ratio undergo greater lateral expansion, resulting in increased horizontal stresses.

The shear modulus diagram illustrates the variations in the reservoir rock in response to applied shear stresses. The graph indicates that the reservoir rock exhibits the highest resistance to shear stresses at both the beginning and end regions, while the lowest resistance is observed in the middle sections of the reservoir (Figure 4).

Figure 5 indicates that the dynamic Young's modulus values exceed the static values, with a linear relationship between the two. The ratio of dynamic Young's modulus to static Young's modulus is typically equal to 1.5 on average. As the Young's modulus of the reservoir rock increases, the difference between these two values decreases, causing their ratio to approach one. For rocks with low moduli, the disparity between these two values is more pronounced, necessitating a larger correction factor.

Uniaxial compressive strength and tensile strength parameters of the reservoir rock are shown in Figure 6.

Modeling the well geomechanics requires two key parameters: rock pore pressure (Pp) and drilling mud weight (Mw). The pore pressure parameter is determined through well testing methods, while the Mw parameter is extracted from daily drilling reports. Figure 7 displays the relationship between pore pressure and mud pressure concerning the well depth.

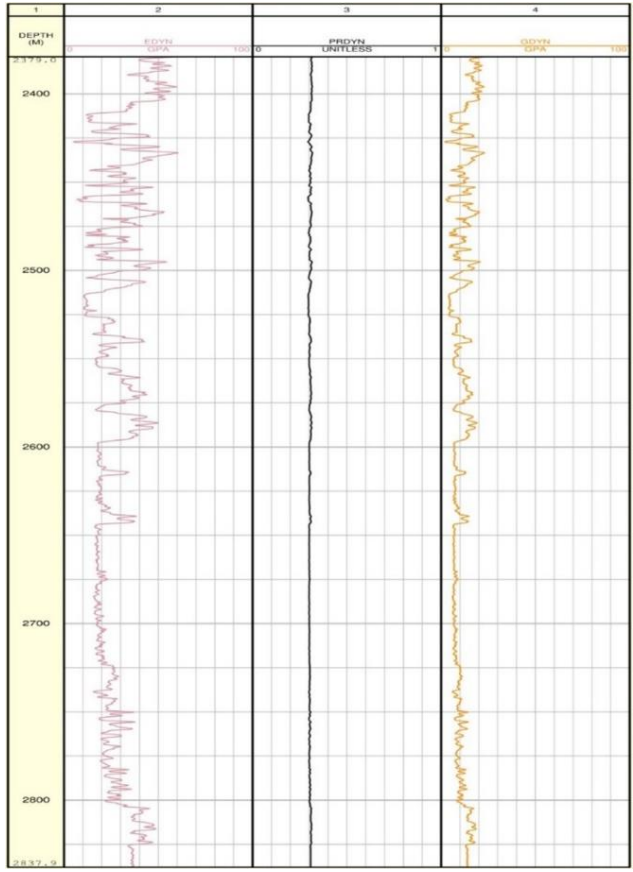


Figure 4. Dynamic elastic moduli of the Asmari reservoir rock in the Ahvaz oil field, as a function of depth

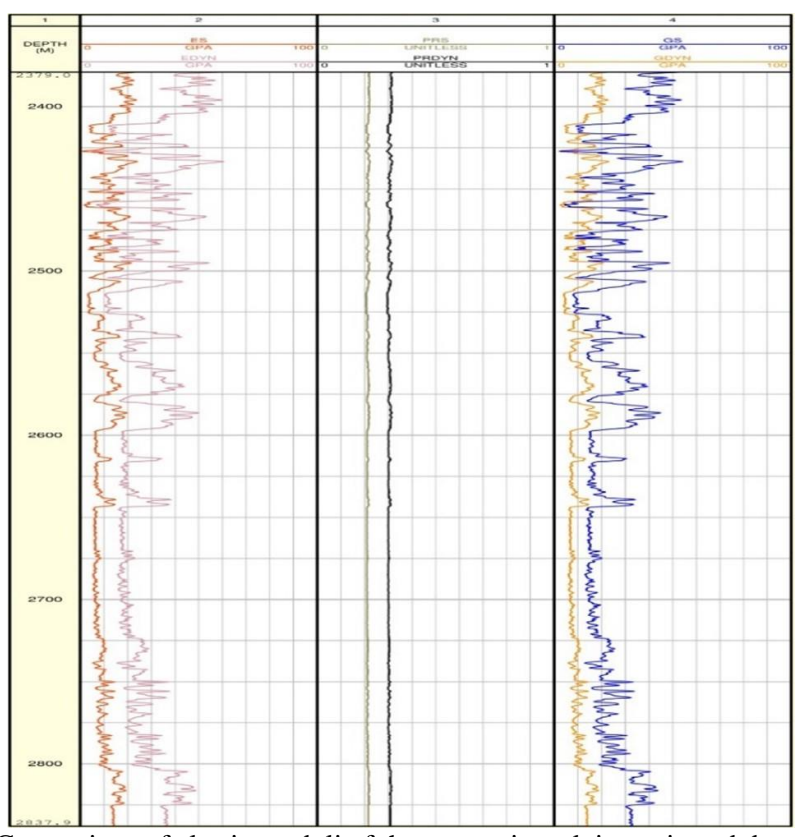


Figure 5. Comparison of elastic moduli of the reservoir rock in static and dynamic modes

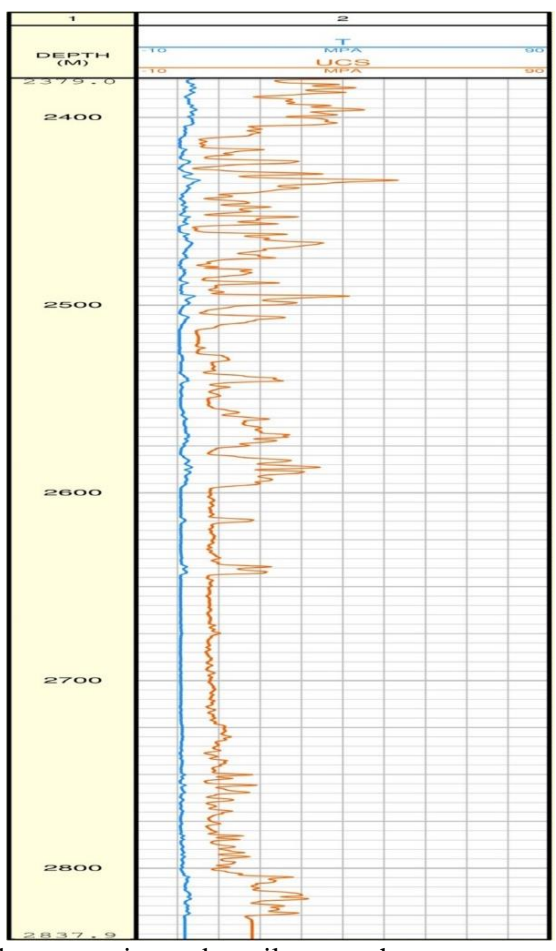


Figure 6. Uniaxial compressive and tensile strength parameters of the reservoir rock



Figure 7. Pore and mud pressure in the reservoir

Calculating the magnitude of the stress field and determining the stress regime

At this stage, it is essential to estimate the principal stress values. In rock mechanics and structural geology, principal stresses are defined as those that exhibit zero shear stress on their acting planes, denoted by the symbols (σ_v , σ_h , and σ_H). The current research employs the fundamental relationships of the stress field to calculate the principal stresses, applying this method to obtain principal stress values at various depths within the studied oil field. The approach is based on dual models that account for the behavior of reservoir rock in both elastic and plastic states, enhancing the accuracy of stress field calculations.

The extracted data required for calculating the principal stresses include the acceleration due to gravity (g), depth (Z), Poisson's ratio (ν), Biot's coefficient (α), pore pressure (Pp), static Young's modulus (Esta), average rock density (RHOBavg), and strain in the x and y directions (ε x and ε y).

A key approach for determining minimum and maximum horizontal stresses is the application of poroelastic relationships, or the surface strain model. In this model, the horizontal stress values can be calculated using overburden pressure, Young's modulus, Poisson's ratio, and horizontal strain values, as presented in the equations below (Fjar et al., 2008).

$$\sigma V = \int_0^z \rho(z) g dz \cong \bar{\rho} g z \tag{6}$$

$$\sigma h = \frac{v}{1 - v} \sigma v - \frac{v}{1 - v} \alpha P p + \alpha P p + \frac{E}{1 - v^2} \varepsilon y + \frac{v E}{1 - v^2} \varepsilon x \tag{7}$$

$$\sigma H = \frac{vsta}{1 - vsta} \sigma v - \frac{vsta}{1 - vsta} \alpha Pp + \alpha Pp + \frac{Esta}{1 - vsta^2} \varepsilon x + \frac{vstaEsta}{1 - vsta^2} \varepsilon y$$
 (8)

Biot's coefficient (α) is typically determined through laboratory tests, with values ranging from zero for hard rocks with no porosity to one for porous rocks in shallow sedimentary basins. The Biot coefficient indicates changes in porosity and permeability in the reservoir rock and its value is between 0 and 1. The more porous and permeable the rock, the value goes towards 1. Poisson's ratio also shows changes in length to width of the rock against stress, which indicates the ductility of the rock.

In this research, the values are set as follows: $\alpha = 1$, $\varepsilon_x = 1.5$, and $\varepsilon_{\gamma} = 0.5$. Figure 8 depicts the stresses obtained at different depths.

The resulting graph of in situ stresses allows for a comparative analysis to determine the stress regime present within the reservoir. Anderson presented three types of stress regimes using the Mohr-Coulomb failure theory. Anderson's classification describes fault regimes based on the direction and relative amounts of three main stresses (Hashemi et al. 2014).

The three primary stress components acting within the Earth's crust are vertical stress (S_v) , maximum horizontal stress (S_H) , and minimum horizontal stress (S_h) . These stress components give rise to three distinct types of stress regimes in the subsurface environment.

Figure 8 indicates that the vertical stress exceeds the maximum horizontal stress, which in turn is greater than the minimum horizontal stress, as represented by the inequality ($S_v > S_H > S_h$). This shows a normal stress regime throughout the reservoir, with the prevailing fault type being a normal fault.

In the initial areas of the reservoir, the values of the three stress components are nearly equal, resulting in well stability that is consistent and optimal in all directions and azimuths. In other words, the well can be inclined in any desired direction. However, in the middle and end regions of the reservoir, the two horizontal stresses are nearly equal but significantly differ from the vertical stress. Consequently, the optimal drilling path aligns with and runs parallel to the vertical stress.

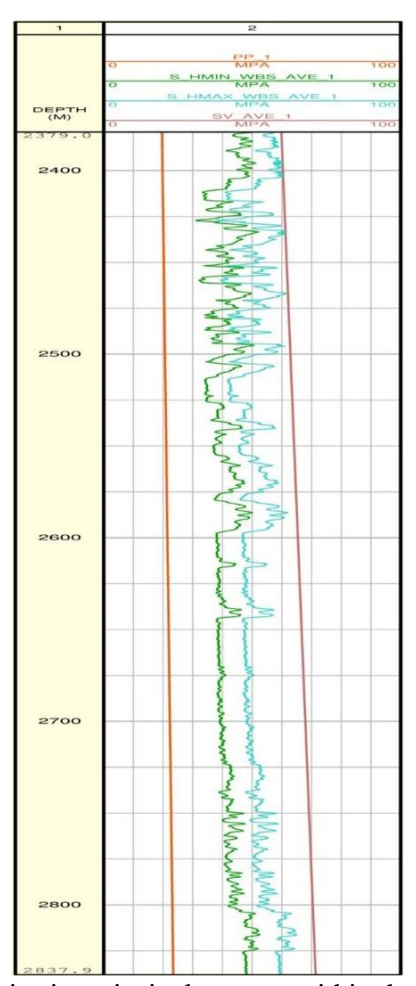


Figure 8. in situ principal stresses within the reservoir

Determining the orientation of stresses using the caliper log and image log

In the oil industry, drilling tools are utilized to gather information about the extent and dip of stratification, as well as the size and diameter of the drilled well. Geological complexities are assessed using two orientations: vertical (straight) and dip parameters (Bozorgi et al., 2016).

For the studied well, the data from the six-arm caliper log were analyzed to determine the orientation of the stresses in the field, and the results are presented in Figure 9. The rose flower diagram depicting the locations of collapse indicates the orientation of the minimum horizontal in situ stress is N19W (Figure 10). As mentioned earlier, the orientation of the maximum horizontal in situ stress is perpendicular to that of the minimum horizontal stress.

Imaging tools generate images of the well environment by measuring variations in the electrical resistance of the surrounding environment. Shear fractures of the wellbore, resulting from in situ stresses, lead to an increase in the well's diameter in a specific direction. This phenomenon, in turn, causes the drilling mud to fill the gap between the resistance sensor and the wellbore (Almalikee and Al-Najim, 2018).

Therefore, the tool measures the resistance of the drilling mud rather than that of the well wall. In the well, the drilling mud used is of the water-based type. In other words, the tool shows high conductivity in areas of wall shear deformation (BB), which exhibit a phase difference of 180 degrees at a specific depth (Gholami et al., 2017). The well features image log charts (XRMI) in the 1.2- to 8-inch hole, which demonstrate high quality and accuracy. To determine the orientation of the principal horizontal stresses, visual diagrams were meticulously analyzed using Techlog software to identify shear failure (wall collapse) and induced failure. The XRMI

image diagram of the well, along with the six-arm diametric diagram, is partially presented in Figures 11 and 14 to identify the areas of shear failure (wellbore collapse).

The results of examining the orientation of the principal in situ horizontal stresses are presented in an image log from the 1.2- to 8-inch open hole of the well (C) (Figure 13).

The orientation of the wellbore (BO) collapse is measured at 161-341 in the first part and 166-346 degrees in the second part of the image log (Figures 13 and 14).

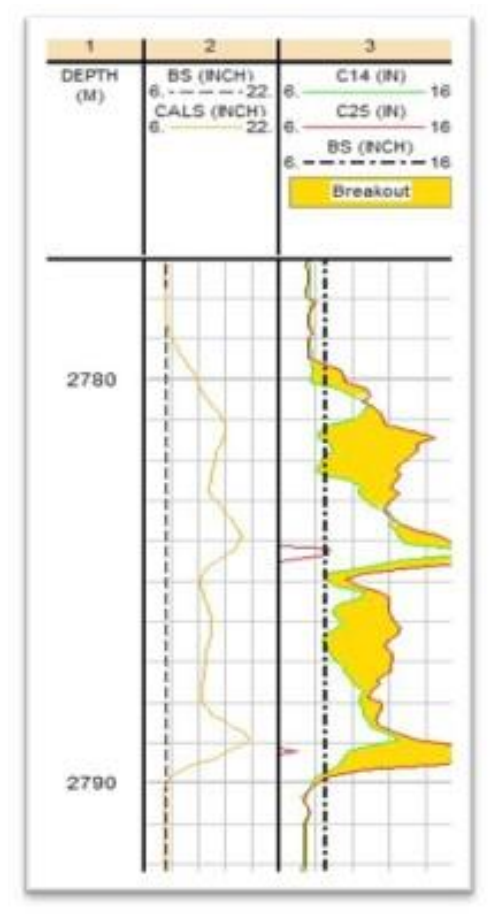


Figure 9. Charts displaying the depth, bit size, and wellbore diameter, along with the drop zone within the well

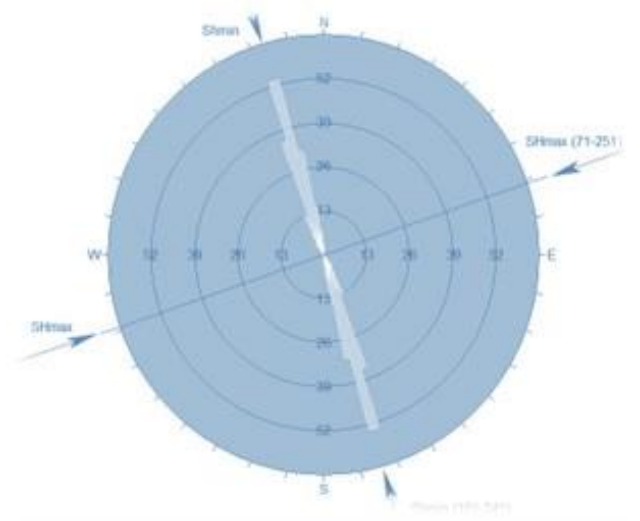


Figure 10. The rose diagram of the caliper log illustrating the diameter and length to determine the orientation of the minimum horizontal stress within the well

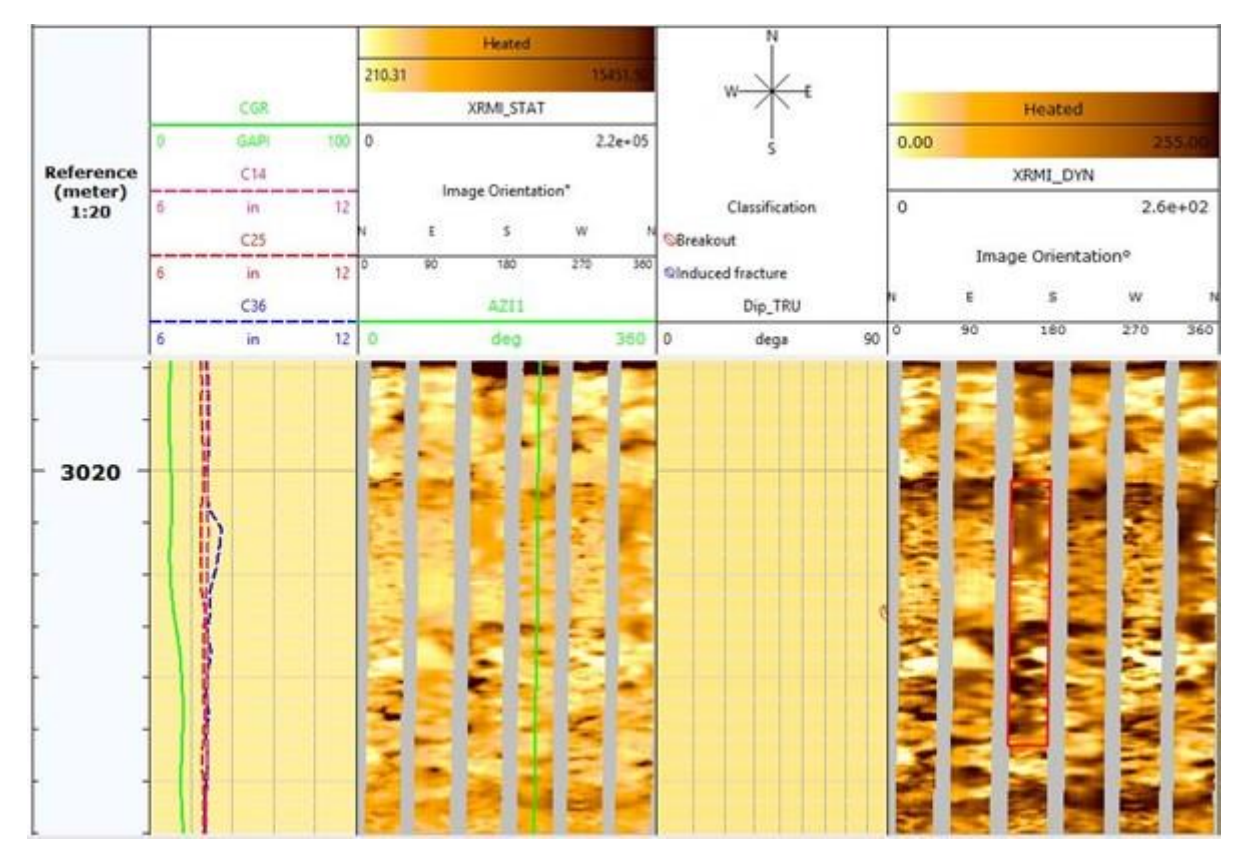


Figure 11. Identification of the areas of shear failure (wall collapse) in a section of the 1.2- to 8-inch open hole of the well

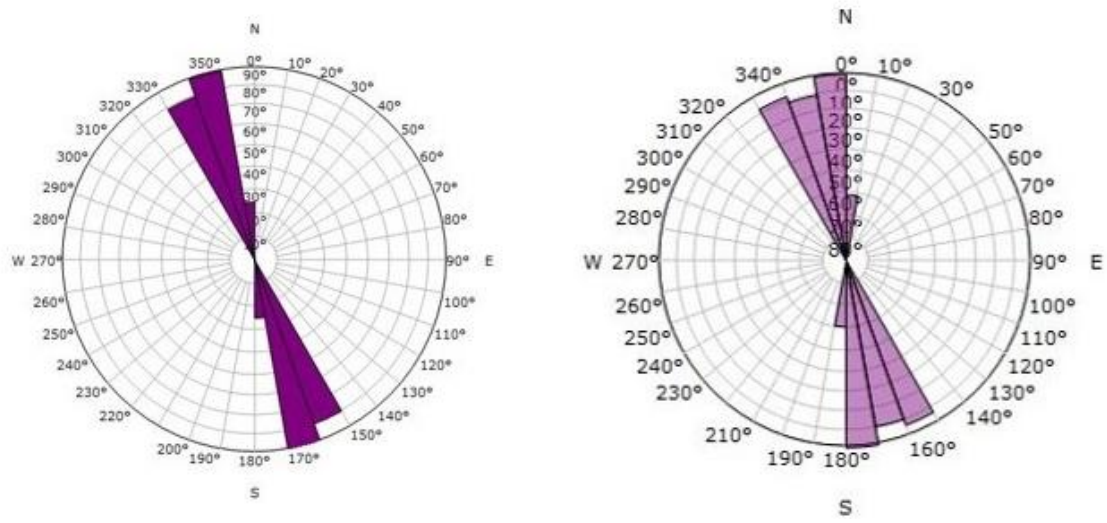


Figure 12. The rose diagram depicting the orientation of minimum horizontal stress (σ h) in the first part (left) and second part (right) of the image log of the well

In addition to shear fractures accompanied by wall thickening, tensile fractures induced by drilling within the wellbore serve as another valuable and common indicator for assessing the magnitude of the principal horizontal in situ stresses. These fractures form on the wellbore wall when the concentration of stress increases to a level sufficient to induce a tensile fracture (Rahimi, 2014). These types of fractures typically occur in vertical wells and are oriented parallel to the well axis. As explained earlier, maximum stress concentration occurs in the direction of minimum horizontal stress, which leads to shear ruptures in the wellbore. However, the initial tensile fracture in the well wall occurs in the direction with the lowest stress concentration when the pressure within the well is generated by drilling into the rock. Since the

direction of the maximum horizontal in situ stress is in line with the minimum stress concentration, the induced fractures resulting from drilling occur in the direction of the maximum horizontal in situ stress. Figure 14 displays some induced tensile fractures in the wellbore.

Rose diagrams of tensile fractures (DIFs) identified in the 1.2 to 8-inch open hole of the studied field (Figure 15).

Determining the average direction of maximum in situ horizontal stress (σH)

Based on the equations proposed by Marbia (1972), the orientation of BO and DIF is represented by the angle θ i. Angles ranging from 180 to 360 degrees are equivalent to 0-180 degrees. The angle for performing calculations is defined in degrees using Equation 10.

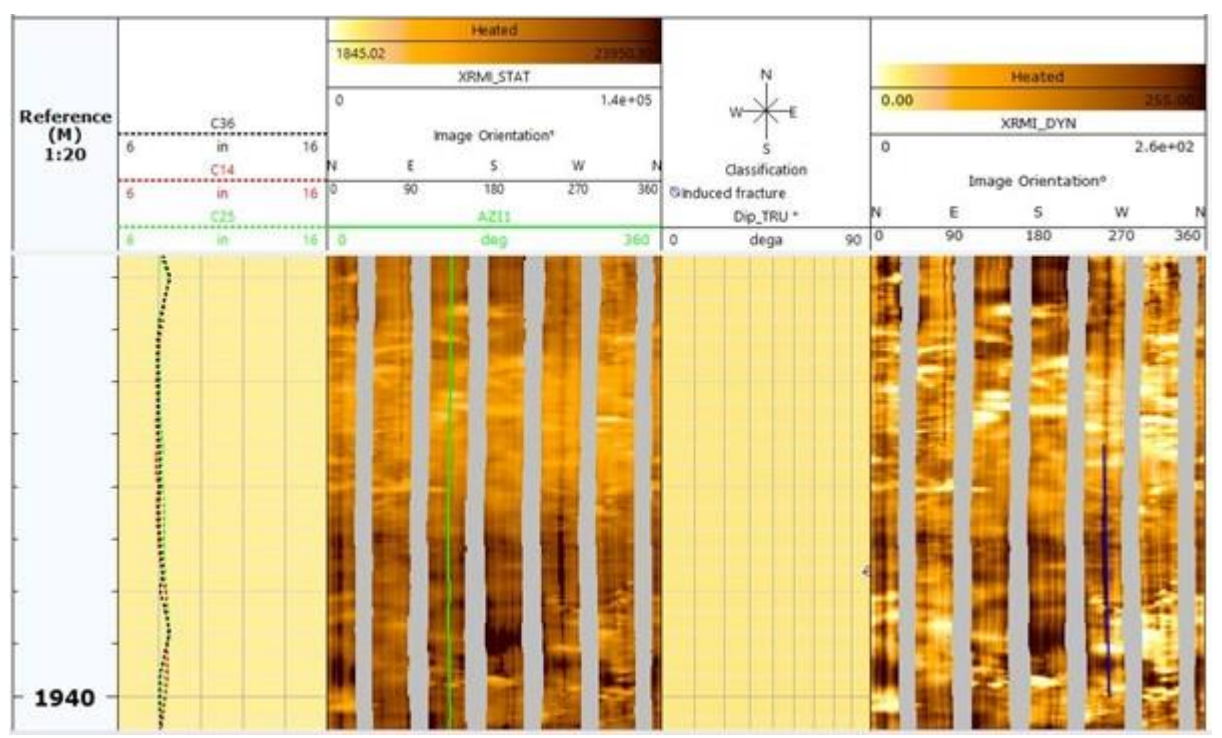


Figure 13. Areas of induced tensile fractures in a section of the 1.2- to 8-inch open hole of the well (C)

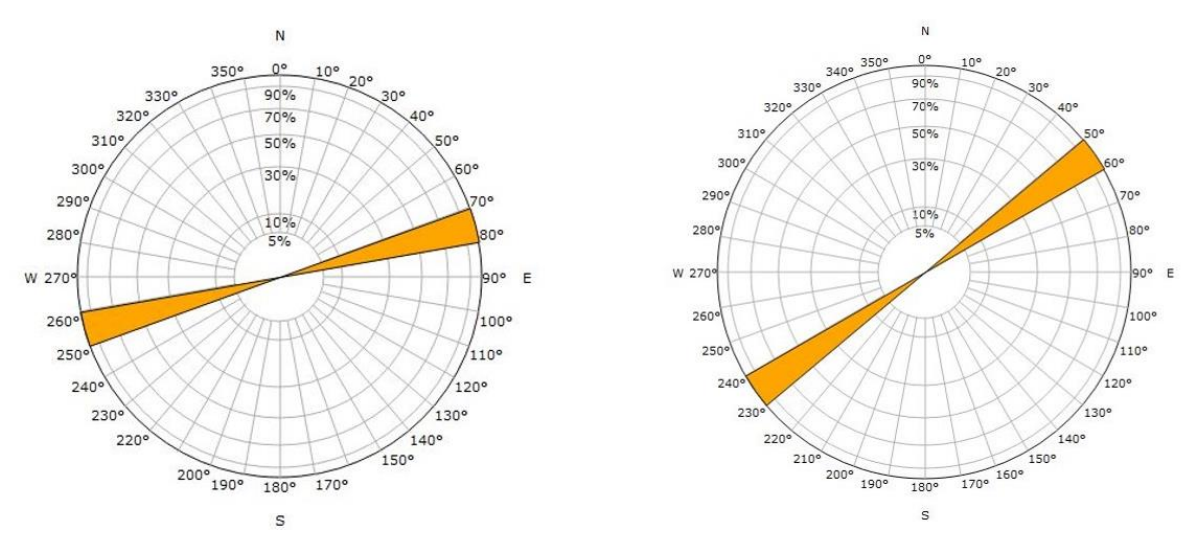


Figure 14. Rose diagrams illustrating the orientation of maximum horizontal stress orientation (σ H) in the first part (left) and second part (right) of the image log of the well

$$\theta_i^* = 2\theta \tag{10}$$

A maximum of two numerical longitudinal and weighting methods are employed to determine the average direction of the horizontal in-situ stress. These two methods are summarized in Table 2.

It should be noted that θm represents the average minimum horizontal in situ stress direction. The calculated results of the parameters in Table 2 for the studied well are presented in Table 3.

Table 2. Numerical and longitudinal weight method parameters to determine the average direction of the maximum in situ stress

Longitudinal weig	ht method	Numerical weight	method
L	total length	n	Number
$\frac{1}{L}\sum_{i=1}^{n}l_{i}cos\theta_{i}^{*}$	Parameter C	$\frac{1}{n}\sum_{i=1}^{n}\cos\theta_{i}^{*}$	Parameter C
$\frac{1}{L}\sum_{i=1}^{n}l_{i}\sin\theta_{i}^{*}$	Parameter S	$\frac{1}{n}\sum_{i=1}^{n}\sin\theta_{i}^{*}$	Parameter S
$\frac{1}{2} \operatorname{arctan}(^{S}/_{\mathbb{C}})$	θ_{m}	$\frac{1}{2} \operatorname{arctan}(S/C)$	θ_{m}
$(C^2 + S^2)^{\frac{1}{2}}$	Parameter R	$(C^2 + S^2)^{\frac{1}{2}}$	Parameter R
$\frac{360}{2\pi} \left(-\frac{1}{2} \operatorname{Ln R}\right)^{\frac{1}{2}}$	standard deviation	$\frac{360}{2\pi} \left(-\frac{1}{2} \operatorname{Ln R}\right)^{\frac{1}{2}}$	standard deviation

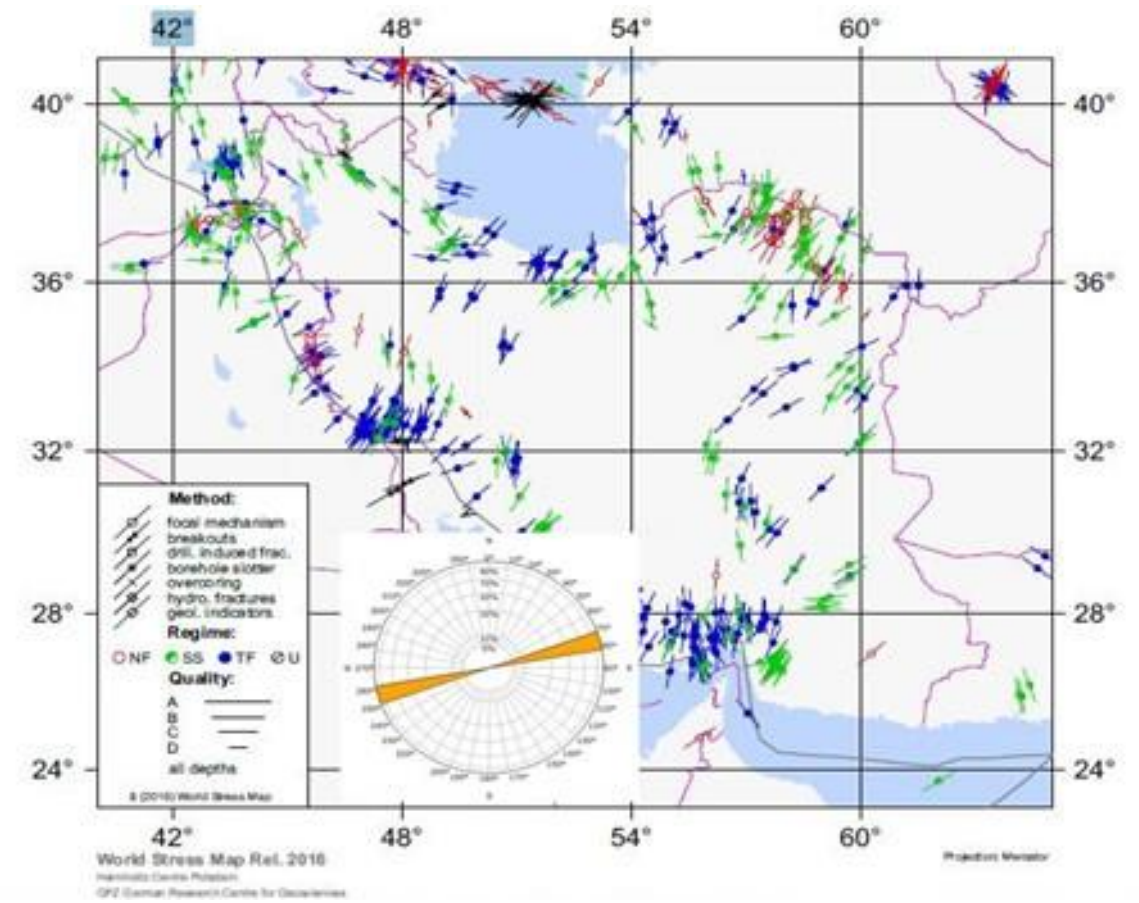


Figure 15. The stress map of Iran, extracted from the World Stress Map (2016), highlighting the investigated field (modified from Heidbach et al., 2018)

According to the results in Table (3), the directions of the minimum and maximum horizontal in situ stresses are N16W-S16E and N74E-S74W, respectively, with a standard deviation of 6.5 degrees. The results of the longitudinal weight method correspond to the rose diagrams in Figures 12 and 14.

Another parameter, known as tectonic regime, is included in the World Stress Map database, along with its corresponding list and symbols. The type of tectonic regime at a given point is determined by evaluating the magnitudes of the in situ horizontal and vertical stresses at that location (Nazeri et al., 2023). The three primary stress regimes are normal fault (NF), strike-slip (SS), and trust fault (TF) regimes. In some cases, where the in-situ stress magnitudes are unknown, the tectonic regime is classified as unknown (U). In the World Stress Map project, the criteria for determining the quality of the maximum in situ horizontal stress direction based on wellbore collapse data are presented in Table 4.

Based on the WSM scoring criteria (Table 4) and the results of the longitudinal weight method calculations (Table 3), the direction and magnitude of the maximum horizontal in situ stress in the well in the investigated field are determined, achieving a score of A. The alignment of the predicted horizontal in situ stresses in the studied well with the stress direction in the Zagros basin was evaluated using the 2016 stress map of Iran, as shown in Figure 16. The investigated field is located at the coordinates of 31° 32' N and 48° 53' E. As shown in Figure 15, the maximum horizontal in situ stress direction calculated for the analyzed field aligns with the stress direction of the Zagros region, indicating a normal stress regime.

Wellbore stability analysis

The concepts of safe mud window and stable mud window for drilling mud are established, and wellbore stability is analyzed in this stage.

As displayed in Figure 16, the safe mud window for drilling mud ranges between Pp and σ 3, while the stable mud window ranges between Min MW and σ 3.

Table 3. Results of the calculations using the numerical and longitudinal weight methods to determine the average direction of the maximum in situ stress

Longitudinal weig	ht method	Numerical weig	ht method
103/15	total length	87	Number
0.825	parameter C	0.816	Parameter C
-0.527	parameter S	-0.523	parameter S
-16.3	$\theta_{ m m}$	-16.3	$\theta_{ m m}$
0.98	parameter R	0.969	parameter R
5/93	standard deviation	7.21	standard deviation

Table 4. Scoring criteria for the World Stress Map (WSM) based on the analysis of shear ruptures in the well wall using the image log tool

Quality- E	Quality- D	Quality - C	Quality- B	Quality- A	parameter
No shedding	Less than 4	more equal to 4	More equal to 6	Greater than or equal to 10	Number of separate drops
-	Less than 20 meters	Greater than or equal to 20 meters	Greater than or equal to 40 meters	Greater than or equal to 100 meters	Total drop length
More than 40	Less than 40	Less than 25	Less than 20	Less than 12	Standard deviation value

Additional results can be derived from this chart, including formation fracture pressure, mud loss zone, breakdown pressure, and formation loss. Figure 17 shows the safe mud window and stability analysis diagram for the studied well.

Prediction of fault activity in the reservoir

Next, the stress path and critical stress path values need to be determined and compared to examine the condition of different layers of the reservoir regarding the potential for fault formation and fracture.

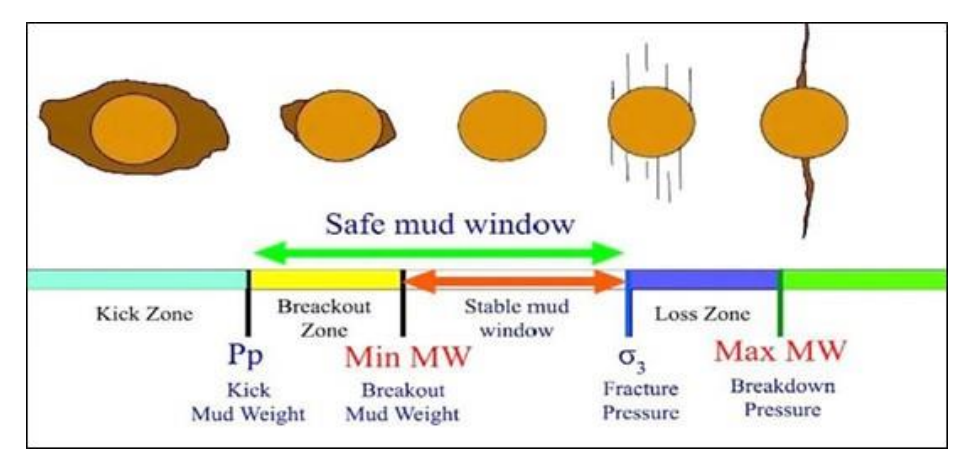


Figure 16. Different ranges of mud windows (modified from Abdideh & Dastyaft, 2022)

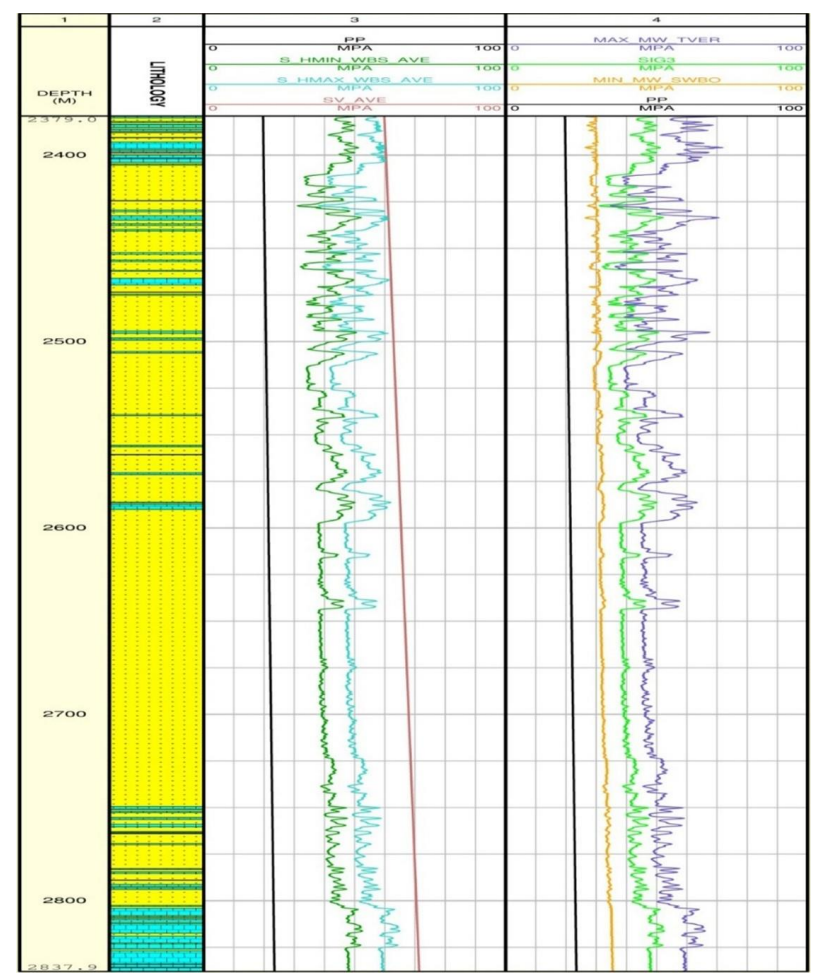


Figure 17. The geomechanical model constructed for a well in the Asmari reservoir, Ahvaz oil field

The stress path and the critical stress path in different areas of the reservoir can be calculated using equations 14 and 15.

The equation of the stress path, which is equal to the ratio of the change in horizontal stress to the change in pore pressure:

$$A = \alpha \left(\frac{1 - 2\nu}{1 - \nu}\right) = \frac{\Delta S Hor}{\Delta P n} \tag{14}$$

where v is the Poisson's ratio and α is Biot's coefficient ($\alpha = 1$).

The equation of the critical stress path is obtained from equation 15:

$$A^* = 1 - \frac{1}{(\sqrt{\mu^2 + 1 + \mu})^2} \tag{15}$$

where μ is the coefficient of rock friction. Values for μ are considered as follows: for sandstone (μ =0.6), for limestone (μ =0.9), and for dolomite (μ =0.8).

Figure 18 shows all areas and ranges of the reservoir where fault formation is possible.

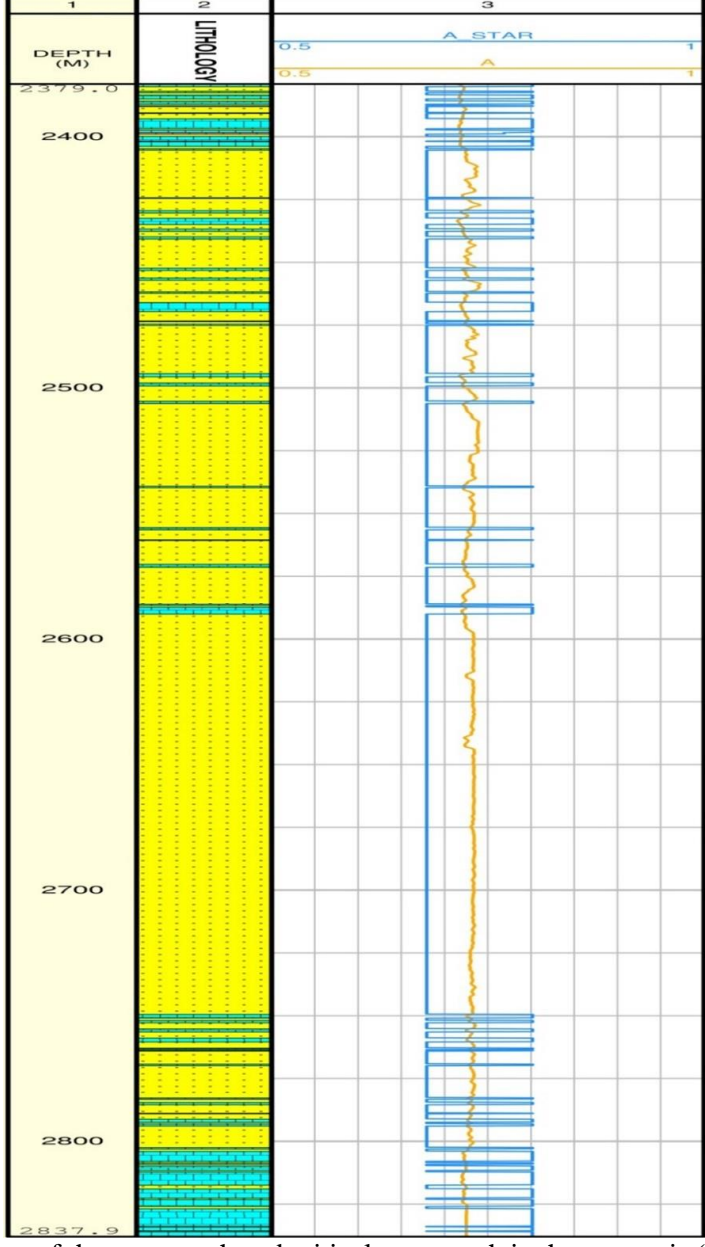


Figure 18. Comparison of the stress path and critical stress path in the reservoir (In the middle areas of the reservoir, where the reservoir rock is sandstone, the values of the stress path parameter are higher than the calculated critical stress path parameter values, which have a high potential for creating new fractures in the reservoir)

In the central areas of the reservoir, particularly in areas where the reservoir rock is sandstone, the values of the stress path parameters exceed those of the calculated critical stress path parameters (Figure 18). Therefore, fault formation is only feasible in the aforementioned areas, while the likelihood of fault development in the remaining areas and layers is minimal, regardless of the production and discharge rates. Draining the reservoir reduces the amount of pore pressure (Pp). If the discharge stress path is greater than its critical value, a normal fault is likely to develop within the reservoir. The existence of a fault during continued drilling or creating a hydraulic fracture can lead to new challenges and issues, such as mud waste. As shown in Figure 18, the probability of fault formation is significantly higher in areas with sandstone formation compared to other areas composed of different reservoir rock materials. The cause of faults in sandstone layers is due to the nature of diagenetic processes, secondary porosity, and permeability of sandstones.

Conclusions

The vertical stress ($\sigma v = Sv$) was calculated to be 60.33 MPa, the minimum horizontal stress ($\sigma h = Sh$) was calculated to be 41.71 MPa, and the maximum horizontal stress ($\sigma H = SH$) was calculated to be 58.66 MPa.

The average uniaxial compressive strength (UCS) was calculated to be 28.49 MPa and the average tensile strength was 2.84 MPa. The pore pressure (Pp) was 19.79 MPa and the mud weight (Mw) was 23.24 MPa.

The safe mud window for drilling mud was calculated for the reservoir, with the loss pressure equivalent to the minimum horizontal stress value (σ 3) averaging approximately 41.75 MPa. The stress regime in the reservoir is classified as a normal fault, and the optimal safe drilling direction in this reservoir is aligned parallel to the vertical stress. The results demonstrate that the minimum and maximum horizontal *in situ* stress directions is N16W-S16E and N74E-S74W, respectively, with a standard deviation of 6.5 degrees.

The stress path value A=0.66 and the critical stress value A*=0.67 were calculated, and given the closeness of these two values with withdrawal from the reservoir and reduction in pore pressure, there is a possibility of normal fault formation in the reservoir.

Fault activity is possible in the sandstone layers of the formation within the studied reservoir; however, the likelihood of fault formation in other layers, such as limestone and dolomite, during the production time is minimal. The formation of faults in the sandstone layers, driven by diagenesis processes, has resulted in increased secondary porosity and permeability due to the creation of additional pore spaces.

Due to the increase in secondary porosity and permeability due to fracturing, the reservoir requires a new production strategy to prevent excessive pressure drop and production loss due to fracturing.

List of symbols

$\vartheta_{ ext{dyn}}$	Dynamic Poisson's Ratio
E _{dyn}	Dynamic Young's Modulus
E _{sta}	Static Young's Modulus
K _{dyn}	Dynamic Bulk Modulus
K _{sta}	Static Bulk Modulus
$V_{\rm p}$	P-Wave Velocity
V_s	S-Wave Velocity
V_{sh}	Shale Volume

Abbreviations

UCS	Uniaxial Compressive Strength
ρ	Density
P	Mud Pressure
P_{p}	Pore Pressure

Statements and declarations

Behrouz Teimouri: Conceptualization, Methodology, Data curation, Software, Writing original draft. Mehran Arian: Supervision and Validation. Mohammad Abdideh: Conceptualization, Visualization, Ali Solgi and Zaha Maleki Investigation, Writing review & editing. We have no conflict of interest to declare. This statement is to certify that all Authors have seen and approved the manuscript being submitted. We warrant that the article is the Authors' original work. We warrant that the article has not received prior publication and is not under consideration for publication elsewhere.

References

- Abdelghany, W.K., Hammed, M., Radwan, A.E., 2023. Implications of machine learning on geomechanical characterization and sand management: a case study from Hilal field, Gulf of Suez: Egypt: Journal of Petroleum Exploration and Production Technology, 13(1): 297-312.
- Abdelghany, W.K., Radwan, A.E., Elkhawaga, M.A., Wood, D.A., S. S., Kassem, A.A., 2021. Geomechanical modeling using the depth of-damage approach to achieve successful underbalanced drilling in the Gulf of Suez rift basin: Journal of Petroleum Science and Engineering, 202:108311.
- Abdideh, M., Dastyaft, F., 2022. Stress field analysis and its effect on selection of optimal well trajectory in directional drilling (case study: southwest of Iran): Journal of Petroleum Exploration and Production Technology, 12(3): 835-849.
- Allahkarampour, D.M., Seyrafian, A., Vaziri-Moghaddam, H. 2010. The Asmari Formation, north of the Gachsaran (Dill anticline), southwest Iran: facies analysis, depositional environments and sequence stratigraphy; Carbonates and Evaporates, 25:145-160
- Almalikee, H.S.A., Al-najim, F.M.S., 2018. Overburden stress and pore pressure prediction for the North Rumaila oil field: Modeling Earth Systems and Environment, 4(3): 1181-1188.
- Anees, A., Zhang, H., Ashraf, U., Wang, R., Liu, K., Mangi, H.N., Jiang, R., Zhang, X., Liu, Q., Tan, S., Shi, W. 2022. Identification of Favorable Zones of Gas Accumulation via Fault Distribution and Sedimentary Facies: Insights From Hangjinqi Area, Northern Ordos Basin: Frontiers in Earth Science, 9: 822670.
- Arian, M., Bagha, N., Khavari, R., Noroozpour, H., 2012. Seismic sources and neo-tectonics of Tehran area (North Iran): Indian Journal of Science and Technology, 5(3): 2379-2383.
- Ashena, R., Elmgerbi, A., Rasouli, V., Ghalambor, A., Rabiei, M., Bahrami, A. 2020. Severe wellbore instability in a complex lithology formation necessitating casing while drilling and continuous circulation system: Journal of Petroleum Exploration and Production Technology, 10(4):1511-1532.
- Ashena, R., Roohi, A., Ghalambor, A. 2022. Wellbore stability analysis in an of shore high-pressure high-temperature, gas field revealed lost times due to lack of well trajectory optimization. SPE Int Conf Exhibit Format Damage Control. https://doi.org/10.2118/208864-MS.
- Ashraf, U., Zhang, H., Anees, A. 2024. Assessment of lake-level variations to decipher geological controlling factors and depositional architecture of Lake Fuxian, Yunnan Plateau: preliminary insights from geophysical data: Geomechanics and Geophysics for Geo-Energy and Geo-Resources, 10: 64.
- Azadpour, M., Shad Manaman, N., Kadkhodaie-Ilkhchi, A., Sedghipour, M.R. 2015. Pore pressure prediction and modeling using well logging data in one of the gas fields in south of Iran: Journal of Petroleum Science and Engineering ,128:15-23.
- Bagheri, H., Tanha, A.A., Doulati Ardejani, F., Heydari-Tajareh, M., Larki, E. 2021. Geomechanical

model and wellbore stability analysis utilizing acoustic impedance and reflection coefficient in a carbonate reservoir: Journal of Petroleum Exploration and Production Technology, 11(11): 3935-3961.

- Bashmagh, N.M., Lin, W., Murata, S., Yousef, F., Radwan, A.E. 2022. Magnitudes and orientations of present-day in-situ stresses in the Kurdistan region of Iraq: insights into combined strike-slip and reverse faulting stress regimes: Journal of Asian Earth Sciences, 239:105398.
- Berberian, M. 1995. Master "blind" thrust faults hidden under the Zagros folds: active basement tectonics and surface morphotectonics, Tectonophysics, 241(3): 193-224
- Darvishpour, A., Seifabad, M.C., Wood, D.A., Ghorbani, H. 2019. Wellbore stability analysis to determine the safe mud weight window for sandstone layers: Petroleum Exploration and Development, 46(5): 1031-1038.
- Edress, N.A., Darwish, S., Ismail, A., 2021. Geochemical characterization of the source rock intervals, beni-suef basin, west nile valley, Egypt: Open Geosciences, 13(1): 1536-1551.
- Farsimadan, M., Dehghan, A.N., Khodaei, M. 2020. Determining the domain of in situ stress around Marun Oil Field's failed wells, SW Iran: Journal of Petroleum Exploration and Production Technology, 10: 1317-1326.
- Fjar, E., Holt, R.M., Horsrud, P., Raaen, A.M., Risnes, R. 2008. geological aspects of petroleum related rock mechanics: Developments in petroleum science, 53: 103-133.
- Gholami, R., Aadnoy, B., Foon, L.Y., Elochukwu, H. 2017. A methodology for wellbore stability analysis in anisotropic formations: a case study from the Canning Basin, Western Australia: Journal of Natural Gas Science and Engineering, 37: 341-360.
- Han, Y., Liu, C., Phan, D., Alruwaili, K., Abousleiman, Y. 2019. Advanced wellbore stability analysis for drilling naturally fractured rocks. In: SPE middle east oil and gas show and conference. https://doi. org/10.2118/195021-MS.
- Hashemi. S.S., Taheri, A., Melkoumian, N. 2014. Shear failure analysis of a shallow depth unsupported borehole drilled through poorly cemented granular rock: Engineering geology, 183: 39-52.
- Heidbach, O., Rajabi, M., Cui, X., Fuchs, K., Müller, B., Reinecker, J., Reiter, K., Tingay, M., Wenzel, F., Xie, M. O., Ziegler, M.-L., Zoback, M., Zoback 2018. The World Stress Map database release 2016: Crustal stress pattern across scales: Tectonophysics, 744: 484-498.
- Hoseinpour, M., Riahi, M.A. 2022. Determination of the mud weight window, optimum drilling trajectory, and wellbore stability using geomechanical parameters in one of the Iranian hydrocarbon reservoirs: Journal of Petroleum Exploration and Production Technology, 12(1): 63-82.
- Hosseini, E., Neshat Ghojogh, J., & Habibnia, B. 2015. Characterization of fractures of Asmari Formation by using image logs, case study: Marun Oilfield: American Journal of Oil and Chemical Technologies, 3(5): 45-47.
- Khodami, E., Ramezanzadeh, A., Sharifi, A. 2021. The 3D simulation of the effect of casing standoff on cement integrity by considering the direction of horizontal stresses in one of the wells of Iranian oil fields, Journal of Petroleum Science and Engineering, 206: 108980.
- Mohammed, H.Q. 2017. Geomechanical analysis of the wellbore instability problems in Nahr Umr Formation southern Iraq. Missouri University of Science and Technology. https://scholarsmine.mst. Edu/masters theses/7695 Mondal S,
- Najafi, M., Lajmorak, S. 2020. Contractional salt-tectonic system in the south Dezful embayment, Zagros: Journal of Structural Geology, 141: 104204
- Nazeri, S., Abdi, F., Ismail, A.,2023. Earthquake source parameters in Zagros region (Iran) from the time-evolutive P-wave displacement: Scientific Reports 13: 17964.
- Qing, L., Shi-hao, L., Weize, M., Yang, Y., Xu, L. 2024. A numerical simulation-based ANN method to determine the shear strength parameters of rock minerals in nanoscale: Computers and Geotechnics, 169: 106175.
- Radwan, A., Sen, S. 2021. Stress Path Analysis for Characterization of In Situ Stress State and Effect of Reservoir Depletion on Present-Day Stress Magnitudes: Reservoir Geomechanical Modeling in the Gulf of Suez Rift Basin, Egypt: Natural Resources Research, 30: 463-478.
- Rahimi, R. 2014. The effect of using different rock failure criteria in wellbore stability analysis. Missouri University of Science and Technology. Missouri University of Science and Technology ProQuest Dissertations & Theses, 1561248.
- Sherkati, Sh., Molinaro, M., Frizon de Lamotte D., Letouzey, J. 2005. Detachment folding in the Central

- and Eastern Zagros fold-belt (Iran): salt mobility, multiple detachments and late basement control: Journal of Structural Geology, 27 (9): 1680-1696.
- Shraf, U., Hucai, Z., Aqsa, A., Muhammad, A., Xiaonan, Z., Saiq, S. Hassan, N. 2020.Controls on Reservoir Heterogeneity of a Shallow-Marine Reservoir in Sawan Gas Field, SE Pakistan: Implications for Reservoir Quality Prediction Using Acoustic Impedance Inversion: Water 12(11): 2972
- Taghipour, M., Ghafoori, M., Lashkaripour, G. R. 2021. A Geomechanical Evaluation of Fault Reactivation Using Analytical Methods and Numerical Simulation: Rock Mechanics and Rock Engineering,54: 695-719.
- Yifan, C, Y., Wanting, H., José, M. C., Wubing, D., Zhiwei, W. 2024. Thermo-poroelastic AVO modeling of Olkaria geothermal reservoirs: Geoenergy Science and Engineering: 241: 213166.

